

Computing nonsimple polygons of minimum perimeter

Journal Article

Author(s):

Fekete, Sándor P.; Haas, Andreas; Hemmer, Michael; Hoffmann, Michael; Kostitsyna, Irina; Krupke, Dominik; Maurer, Florian; Mitchell, Joseph S.B.; Schmidt, Arne; Schmidt, Christiane; Troegel, Julian

Publication date:

2017

Permanent link:

<https://doi.org/10.3929/ethz-b-000229763>

Rights / license:

[Creative Commons Attribution 4.0 International](#)

Originally published in:

Journal of Computational Geometry 8(1), <https://doi.org/10.20382/jocg.v8i1a13>

COMPUTING NONSIMPLE POLYGONS OF MINIMUM PERIMETER*

Sándor P. Fekete,[†] Andreas Haas,[†] Michael Hemmer,[†] Michael Hoffmann,[‡]
Irina Kostitsyna,[§] Dominik Krupke,[†] Florian Maurer,[†] Joseph S. B. Mitchell,[¶]
Arne Schmidt,[†] Christiane Schmidt,^{||} Julian Troegel[†]

ABSTRACT. We consider the Minimum Perimeter Polygon Problem (MP3): for a given set V of points in the plane, find a polygon P with holes that has vertex set V , such that the total boundary length is smallest possible. The MP3 can be considered a natural geometric generalization of the Traveling Salesman Problem (TSP), which asks for a *simple* polygon with minimum perimeter. Just like the TSP, the MP3 occurs naturally in the context of curve reconstruction.

Even though the closely related problem of finding a minimum cycle cover is polynomially solvable by matching techniques, we prove how the topological structure of a polygon leads to NP-hardness of the MP3. On the positive side, we provide constant-factor approximation algorithms.

In addition to algorithms with theoretical worst-case guarantess, we provide *practical* methods for computing provably optimal solutions for relatively large instances, based on integer programming. An additional difficulty compared to the TSP is the fact that only a subset of subtour constraints is valid, depending not on combinatorics, but on geometry. We overcome this difficulty by establishing and exploiting geometric properties. This allows us to reliably solve a wide range of benchmark instances with up to 600 vertices within reasonable time on a standard machine. We also show that restricting the set of connections between points to edges of the Delaunay triangulation yields results that are on average within 0.5% of the optimum for large classes of benchmark instances.

1 Introduction

Two of the most fundamental structures in Computational Geometry are planar point sets and polygons. In this paper we study a natural algorithmic connection between them. For

*A preliminary extended abstract [13] appeared in the Proceedings of the 15th Symposium on Experimental and Efficient Algorithms (SEA 2016).

[†]Department of Computer Science, TU Braunschweig, Mühlenpfordtstr. 23, 38106 Braunschweig, Germany. {s.fekete,a.haas,m.hemmer,d.krupke,arne.schmidt,j.troegel}@tu-bs.de

[‡]Department of Computer Science, ETH Zürich, Universitätstrasse 6, 8092 Zürich, Switzerland. hoffmann@inf.ethz.ch

[§]Department of Mathematics and Computer Science, TU Eindhoven, 5600 MB Eindhoven, The Netherlands. i.kostitsyna@tue.nl

[¶]Department of Applied Mathematics and Statistics, Stony Brook University, Stony Brook, NY 11794-3600, USA. joseph.mitchell@stonybrook.edu

^{||}Department of Science and Technology, Linköping University, SE 60174 Norrköping, Sweden. christiane.schmidt@liu.se

a given set V of points in the plane, consider the family of all polygons with holes that have vertex set V . Such a polygon P consists of an exterior boundary that surrounds a collection of interior holes, which are simple disjoint polygonal boundaries with disjoint interior; note that each boundary must contain at least three vertices in order to be non-degenerate.

The Minimum Perimeter Polygon Problem (MP3) asks for a polygon P with holes on vertex set V , such that the total boundary length is smallest possible.



Figure 1: A Minimum Perimeter Polygon for an instance with 960 vertices.

As can be seen from Figure 1, an optimal solution for the MP3 need not be simply connected, but may consist of an outer boundary that surrounds a number of *holes*, i.e., interior boundaries. If holes are disallowed, the problem turns into the well-known Traveling Salesman Problem (TSP): find a shortest polygonal chain through a given set of vertices in the plane. As a consequence of the triangle inequality, any optimal solution of the TSP is always a simple polygon of minimum perimeter.

The TSP is one of the classic problems of Combinatorial Optimization. NP-hard even in special cases of geometric instances (such as grid graphs), it has served as one of the prototypical testgrounds for developing outstanding algorithmic approaches. These include constant-factor approximation methods (such as Christofides' $3/2$ -approximation [7] for metric instances, or Arora's [4] and Mitchell's [23] polynomial-time approximation schemes for geometric instances), as well as exact methods (such as Grötschel's optimal solution to a 120-city instance [16] or the award-winning work by Applegate, Bixby, Chvátal and Cook [2] for solving a 13509-city instance within 10 years of CPU time.) The well-established benchmark library TSPLIB [26] of TSP instances has become so widely accepted that it is used as a benchmark for a large variety of other optimization problems. See the books [17, 21] for an overview of various aspects of the TSP and the books [3, 8] for more details on exact optimization.

Because of the fundamental role of polygons in geometry, the study of TSP solutions has attracted attention for a wide range of geometric applications. One such context is

geometric shape reconstruction, where the objective is to re-compute the original curve from a given set of sample points V ; see Giesen [15], Althaus and Mehlhorn [1] or Dey, Mehlhorn and Ramos [10] for specific examples. However, this only makes sense when the original shape is known to be simply connected, i.e., bounded by a single closed curve. More generally, a shape may be multiply connected, with interior holes. Thus, computing a simple polygon may not yield the desired answer. Instead, the solution may be a Minimum Perimeter Polygon (MPP) on vertex set V . See Figure 1 for an optimal solution of an instance with 960 points; this also shows the possibly intricate structure of an MPP.

While the MP3 asks for a cycle cover of the given set of vertices (as opposed to a single cycle required by the TSP), it is important to note that even the more general geometry of a polygon with holes imposes some topological constraints on the structure of boundary cycles; as a consequence, an optimal 2-factor (a minimum-weight cycle cover of the vertices, which can be computed in polynomial time) may not yield a feasible solution. Fekete et al. [12] gave a generic integer program for the MP3 (and other related problems) that yields optimal solutions for instances up to 50 vertices. However, the main challenges were left unresolved. What is the complexity of computing an MP3? Is it possible to develop constant-factor approximation algorithms? And how can we compute provably optimal solutions for instances of relevant size?

Our Results

In this paper, we resolve the main open problems related to the MP3.

- We prove that the MP3 is NP-hard. This shows that despite of the relationship to the polynomially solvable problem of finding a minimum 2-factor, dealing with the topological structure of the involved cycles is computationally difficult.
- We give a 3-approximation algorithm for the MP3.
- We provide a general IP formulation with $O(n^2)$ variables to ensure a valid solution for the MP3.
- We describe families of cutting planes that significantly reduce the number of iterations needed to eliminate outer components and holes in holes, leading to a practically useful formulation.
- We present experimental results for the MP3, solving instances with up to 1000 points in the plane to provable optimality within 30 minutes of CPU time.
- We also consider a fast heuristic that is based on geometric structure, restricting the edge set to the Delaunay triangulation. Experiments on structured random point sets show that solutions are on average only about 0.5% worse than the optimum, with vastly superior runtimes.

2 Complexity

Theorem 1. *The Minimum Perimeter Polygon Problem (MP3) is NP-hard.*

Proof. The proof is based on a reduction from the Minimum Vertex Cover problem for planar graphs, which was proven to be NP-complete by Garey and Johnson [14]: for an undirected planar graph $G = (V, E)$ and a parameter $k \in \mathbb{N}$, decide whether there exists a subset $V' \subset V$ of at most k vertices such that for every edge $(u, v) \in E$, at least one of u or v is in V' . Given an instance I_{MVC} of the Minimum Vertex Cover problem we construct an instance I_{MP3} of the MP3 such that I_{MP3} has a solution if and only if I_{MVC} has a solution. Given a planar graph G , we replace its vertices with vertex gadgets, connect them with edge gadgets, and add three points at the vertices of a large triangle enclosing the construction. The triangle delimits the outer boundary of the polygon in the instance of the MP3, and the vertex and edge gadgets enforce a choice of cycles covering the points that form the holes of the polygon.

Vertex gadget. The vertex gadget consists of four points (refer to Figure 2). The top three points are always connected by a cycle. If the fourth point p is in the same cycle, that represents putting the corresponding vertex in subset V' . The cycle's length is 3ε if $p \notin V'$, and $2b + 2\varepsilon$ if $p \in V'$.

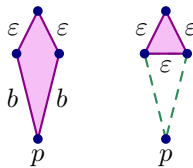


Figure 2: Vertex gadget. Left: $p \in V'$, total length is $2b + 2\varepsilon$; right: $p \notin V'$, total length is 3ε .

Edge gadget. The edge gadget consists of a repeating pattern of four points forming a rhombus (refer to Figure 3). Let some edge gadget consist of r rhombi. There are three ways of covering all the points except for, possibly, the two outermost points, with cycles of total length at most $2ra + r\varepsilon$ (see Figure 3 (a-c)). This will leave either the leftmost point, either the rightmost point, or both, the leftmost and the rightmost points, uncovered by the cycles. If we require both outermost points to be covered by the cycles, their total length is at least $2(r+1)a + (r-1)\varepsilon$ (see Figure 3 (d)). The points of the edge gadget could potentially be covered by a path of length $2ra + r\varepsilon$ (see Figure 3 (e)) that closes into a cycle through other gadgets. To prevent this situation we add triplets of points that form small holes in the middle of each face of G . If a cycle would pass through an edge gadget, then the cycle would enclose at least one face of the graph G and thereby also enclose another hole, which is forbidden.

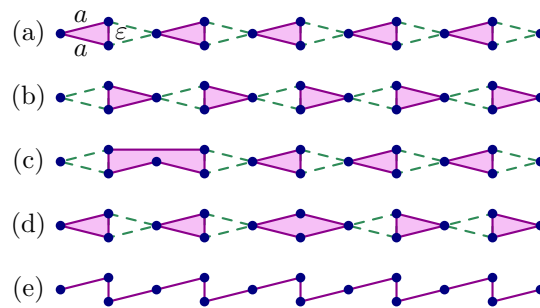


Figure 3: Edge gadget. (a)–(c) the gadget is covered by cycles of total length $\approx 10a + 5\epsilon$; (d) total length $12a + 4\epsilon$; (e) the gadget is covered by a path of total length $10a + 5\epsilon$.

Split gadget. The split gadget (refer to Figure 4) multiplies the connection to a vertex gadget, thus allowing us to connect one vertex gadget to multiple edge gadgets. If point p is covered by the vertex gadget, all the points, including points p_1 and p_2 , of the split gadget can be covered by cycles of total length $16a + 11\epsilon$. If point p is not covered by the vertex gadget, p and all the points of the split gadget, except for p_1 and p_2 , can be covered by cycles of total length $16a + 11\epsilon$. Notice, that the cycles can only consist of the edges that are shown in the figure (with solid or dashed lines). There is always the same number of edges used in any collection of cycles that cover the same number of points. Therefore, if some cycle contains an edge that is longer than a , the other edges in the cycles have to be shorter to compensate for the extra length. By a simple case distinction one can show that there is no collection of cycles of length at most $16a + 11\epsilon$ that covers the same points of the split gadget and that uses any edge that is not shown in Figure 4.

If we require the split gadget to cover points p_1 and p_2 when point p is not covered by the vertex gadget, the total length of the cycles is at least $18a + 10\epsilon$ (see Figure 5).

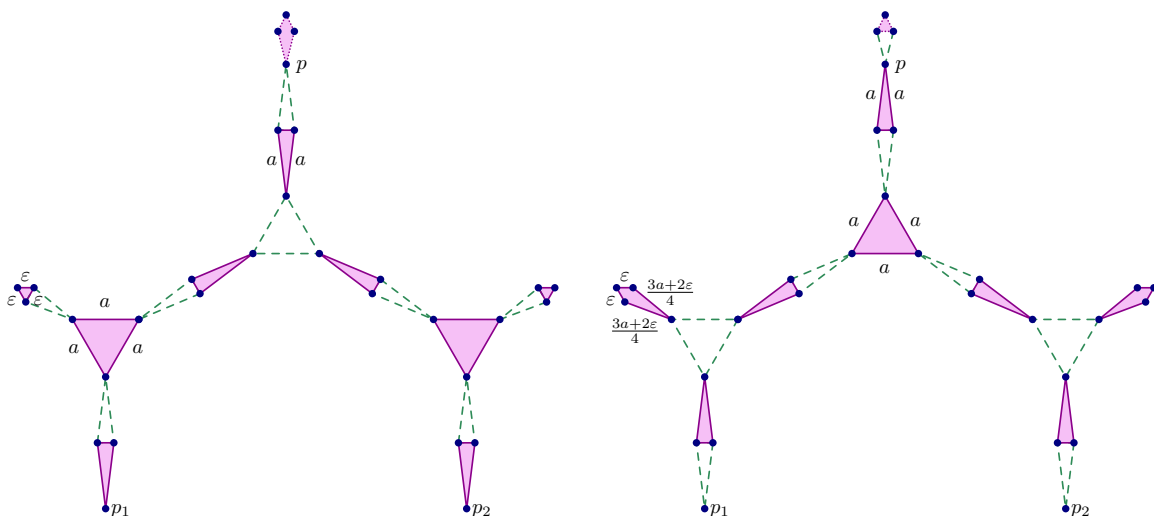


Figure 4: Split gadget. Left: vertex $\in V'$, total length is $16a + 11\epsilon$; right: vertex $\notin V'$, total length is $16a + 11\epsilon$.

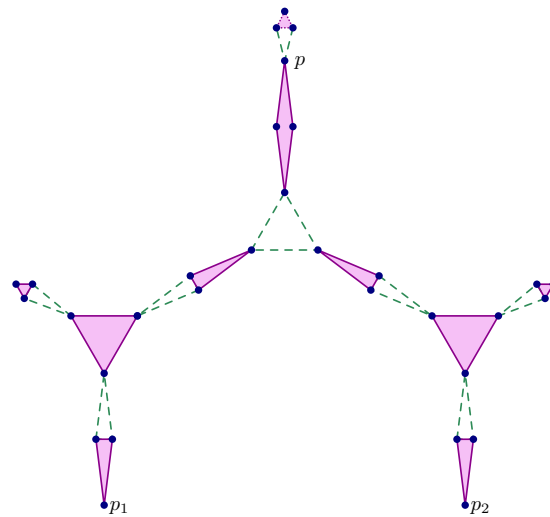


Figure 5: Split gadget: points p , p_1 , and p_2 are covered by cycles of total length $18a + 10\varepsilon$.

To summarize, given an embedding of planar graph $G = (V, E)$ with n vertices and m edges, we construct an instance of the MP3 by replacing the vertices of the graph with the vertex gadgets, attaching $\deg(v) - 1$ split gadgets (where $\deg(v)$ denotes the degree of vertex v) to the corresponding gadget of every vertex v , and connecting the vertex gadgets by edge gadgets (see Figure 6). We enclose the construction in a triangle of a very large size, that will form the outer boundary of the polygon. Let the perimeter of the triangle T be \gg than the diameter of G . The cycles covering the points of the gadgets are the holes in the polygon. Moreover, to every face of G we add triplets of points forming cycles of a very small length $\ll \varepsilon$. This eliminates any possibility of passing through edge gadgets with a single cycle.

The number of vertex gadgets used in the construction is n , and the number of split gadgets is $\sum_{v \in V} \deg(v) - n = 2m - n$. Let the number of rhombi used in all the edge gadgets be r , and let the total length of the extra holes in the middle of the faces of G be ε . Then

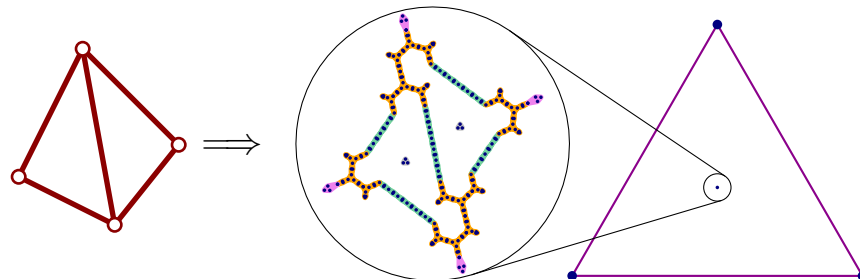


Figure 6: Given a planar graph G , we construct an instance of the MP3. Highlighted in violet are the vertex gadgets, in orange are the split gadgets, in green are the edge gadgets, and in gray are the extra holes in the middle of the faces of G .

the instance of the MP3 asks whether there exists a polygon of perimeter at most

$$\begin{aligned} L &= T + k(2b + 2\varepsilon) + (n - k)3\varepsilon + (2m - n)(16a + 11\varepsilon) + 2ra + r\varepsilon + \varepsilon \\ &= (2b - \varepsilon)k + T + 2(16m - 8n + r)a + (22m - 8n + r + 1)\varepsilon. \end{aligned}$$

Let d be the length of the shortest edge. Choose a , b , and ε , such that $\varepsilon \ll b \ll a \ll d$. Using standard graph embedding techniques, it is straightforward to see that all coordinates of this embedding are polynomial in the size of the original graph.

Then there is a polygon with perimeter at most L for I_{MP3} if and only if there is a vertex cover of size at most k for I_{MVC} .

Let V' be a vertex cover of size k of $G = (V, E)$. Then, by selecting the corresponding vertex gadgets to cover points p , and propagating the construction of cycles along the split and edge gadgets, we get a polygon of perimeter L .

Let there exist a polygon P with perimeter at most $T + 2(16m - 8n + r)a + 2kb + (22m - 8n + r - k + 1)\varepsilon$. By construction, the outer boundary of P is the triangle of perimeter T . Suppose there are more than k vertex gadgets that are covering the corresponding points p . Then the perimeter of P has to be greater than $T + 2(16m - 8n + r)a + 2kb + (22m - 8n + r - k + 1)\varepsilon$, as the third term (of variable b) of the perimeter expression dominates the fourth term (of variable ε). Thus, there have to be no more than k variable gadgets that cover the corresponding points p . Every edge gadget has to have one of the end-points covered by the vertex gadgets (through split gadgets). Otherwise, the second term of the expression of the polygon perimeter would be greater. Therefore, the polygon corresponds to a vertex cover of size at most k for I_{MVC} . \square

3 Approximation

In this section we show that the MP3 can be approximated within a factor of 3.

Theorem 2. *There exists a polynomial-time 3-approximation algorithm for the MP3.*

Proof. Let OPT be the length of an optimal solution of the MP3 and APX the length of the approximation that our algorithm will compute for the given set, V , of n points in the plane. We compute the convex hull, $CH(V)$, of the input set; this takes time $O(n \log h)$, where h is the number of vertices of the convex hull. Note that the perimeter, $|CH(V)|$, of the convex hull is a lower bound on the length of an optimal solution ($OPT \geq |CH(V)|$), since the outer boundary of any feasible solution polygon must enclose all points of V , and the convex hull is the minimum-perimeter enclosure of V .

Let $U \subseteq V$ be the input points interior to $CH(V)$. If $U = \emptyset$, then the optimal solution is given by the convex hull. If $|U| \leq 2$, we claim that an optimal solution is a simple, not necessarily convex, polygon, with no holes, on the set V , given by the TSP tour on V ; since $|U| = 2$ is a constant, it is easy to compute the optimal solution in polynomial time, by trying all $O(h^2)$ possible ways of inserting the points of U into the cycle of the points of V that lie on the boundary of the convex hull, $CH(V)$.

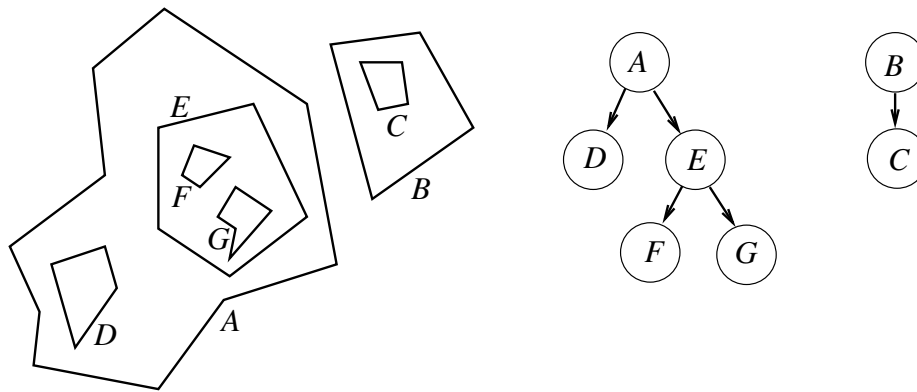


Figure 7: A 2-factor (left) and its corresponding nesting forest (right).

Thus, assume now that $|U| \geq 3$. We compute a minimum-weight 2-factor (i.e., a minimum-weight cycle cover of the vertices), denoted by $\gamma(U)$, on U , which is done in polynomial-time by standard methods [9]. (The time required is that of solving a minimum-weight matching in a bipartite graph having $O(|U|)$ nodes and $O(|U|^2)$ edges; this can be done in time $O(|U|^3)$.) Now, $\gamma(U)$ consists of a set of disjoint simple polygonal curves having vertex set U ; the curves can be nested, with possibly many levels of nesting. We let F denote the directed *nesting forest* whose nodes are the cycles, i.e., the connected components of $\gamma(U)$, and whose directed edges indicate nesting (i.e., containment) of one cycle within another; refer to Figure 7. Since an optimal solution consists of a 2-factor (an outer cycle, together with a set of cycles, one per hole of the optimal polygon), we know that $OPT \geq |\gamma(U)|$. In an optimal solution, the nesting forest corresponding to the set of cycles covering all of V , not just the points U interior to $CH(V)$, is simply a single tree that is a star: a root node corresponding to the outer cycle, and a set of children adjacent to the root node, corresponding to the boundaries of the holes of the optimal polygon. If the nesting forest F for our optimal 2-factor is a set of isolated nodes (i.e., there is no nesting among the cycles of the optimal 2-factor on U), then our algorithm outputs a polygon with holes whose outer boundary is the boundary of the convex hull, $CH(V)$, and whose holes are the disjoint polygons given by the cycles of $\gamma(U)$. In this case, the total weight of our solution is equal to $|CH(V)| + |\gamma(U)| \leq 2 \cdot OPT$.

Assume now that F has at least one nontrivial tree. We describe a two-phase process that transforms the set of cycles corresponding to F into a set of pairwise-disjoint cycles, each defining a simple polygon interior to $CH(V)$, with no nesting. The resulting simple polygons are disjoint, each having at least 3 vertices from $U \subset V$.

Phase 1 of the process transforms the cycles $\gamma(U)$ into a set of polygonal cycles that define *weakly simple* polygons whose interiors are pairwise disjoint, where a polygonal cycle β defines a *weakly simple* polygon P_β if P_β is a closed, simply connected set in the plane with a boundary, ∂P_β consisting of a finite union of line segments, whose traversal (e.g., while keeping the region P_β to one's left) is the counterclockwise cycle β , which can have line segments that are traversed twice, once in each direction. (The notion of a “weakly simple” polygon can have various meanings, which may be slightly different from that used

here; we refer the reader to [5], which includes algorithmic results as well.) The total length of the cycles at the end of phase 1 is at most 2 times the length of the original cycles, $\gamma(U)$. Then, phase 2 of the process transforms these weakly simple cycles into (strongly) simple cycles that define disjoint simple polygons interior to $CH(V)$. Phase 2 only does shortening operations on the weakly simple cycles; thus, the length of the resulting simple cycles at the end of phase 2 is at most 2 times the total length of $\gamma(U)$. At the end of phase 2, we have a set of disjoint simple polygons within $CH(V)$, which serve as the holes of the output polygon, whose total perimeter length is at most $|CH(V)| + 2|\gamma(U)| \leq 3 \cdot OPT$.

We now describe phase 1. Let T be a nontrivial tree of F . Associated with T are a set of cycles, one per node. A node u of T that has no outgoing edge of T (i.e., U has no children) is a sink node; it corresponds to a cycle that has no cycle contained within it. Let v be a node of T that has at least one child, but no grandchildren; clearly, such a node must exist in a nontrivial tree T . Then, v corresponds to a cycle (simple polygon) P_v , within which there is one or more disjoint simple polygonal cycles, $P_{u_1}, P_{u_2}, \dots, P_{u_k}$, one for each of the $k \geq 1$ children of v . We describe an operation that replaces P_v with a new weakly simple polygon, Q_v , whose interior is disjoint from those of $P_{u_1}, P_{u_2}, \dots, P_{u_k}$. Let $e = pq$ ($p, q \in V$) be any edge of P_v ; assume that pq is a counterclockwise edge, so that the interior of P_v lies to the left of the oriented segment pq . Let Γ be a shortest path within P_v , from p to q , that has all of the polygons $P_{u_1}, P_{u_2}, \dots, P_{u_k}$ to its right; thus, Γ is a “taut string” path within P_v , homotopically equivalent to ∂P_v , from p to q . Such a geodesic path is related to the “relative convex hull” of the polygons $P_{u_1}, P_{u_2}, \dots, P_{u_k}$ within P_v , which is the shortest cycle within P_v that encloses all of the polygons; the difference is that Γ is “anchored” at the endpoints p and q . Note that Γ is a polygonal path whose vertices are either (convex) vertices of the polygons P_{u_j} or (reflex) vertices of P_v . The path Γ can be computed in linear ($O(|V|)$) time [18], after triangulating the domain. Consider the closed polygonal walk that starts at p , follows the path Γ to q , then continues counterclockwise around the boundary, ∂P_v , of P_v until it returns to p . This closed polygonal walk is the counterclockwise traversal of a weakly simple polygon, Q_v , whose interior is disjoint from the interiors of the polygons $P_{u_1}, P_{u_2}, \dots, P_{u_k}$. Refer to Figure 8. The length of this closed walk (the counterclockwise traversal of the boundary of Q_v) is at most twice the perimeter of P_v , since the path Γ has length at most that of the counterclockwise boundary ∂P_v , from q to p , because Γ is a homotopically equivalent shortening of this boundary. We consider the boundary of P_v to be replaced with the cycle around the boundary of Q_v , and this process has reduced the degree of nesting in T : node v that used to have k children (leaves of T) is now replaced by a node v' corresponding to Q_v , and v' and the k children of v are now all siblings in the modified tree, T' . If v had a parent, w , in T , then v' and the k children of v are now children of w ; if v had no parent in T (i.e., it was the root of T), then T has been transformed into a set of $k + 1$ cycles, none of which are nested within another cycle of $\gamma(U)$; each is within the convex hull $CH(V)$, but there is no other surrounding cycle of $\gamma(U)$. We continue this process of transforming a surrounding parent cycle (node v) into a sibling cycle (node v'), until each tree T of F becomes a set of isolated nodes, and finally F has no edges, i.e., there is no nesting.

Phase 2 is a process of local shortening of the cycles/polygons, Q_1, Q_2, \dots, Q_m , that resulted from phase 1, in order to remove repeated vertices in the weakly simple cycles, so

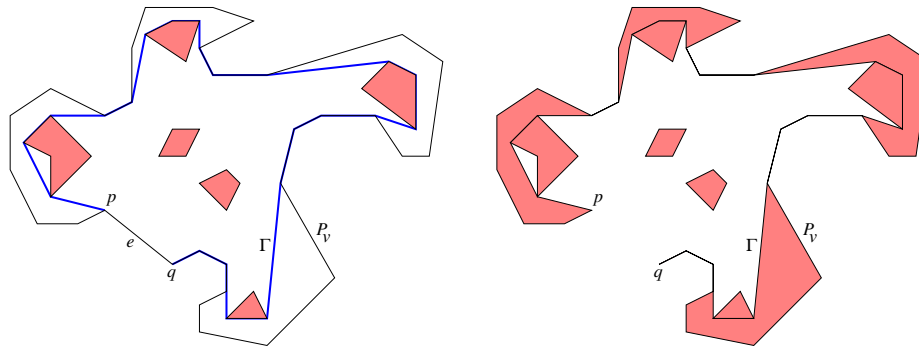


Figure 8: Left: The geodesic path Γ from p to q within P_v , surrounding all of the (red) polygons $P_{u_1}, P_{u_2}, \dots, P_{u_k}$. Right: The new weakly simple polygon (now red) obtained from the traversal of Γ and the boundary of P_v .

that cycles become strongly simple. There are two types of repeated vertices to resolve: those that are repeated within the same cycle, i.e., repeated vertices p of a cycle Q_i where ∂Q_i “pinches” upon itself, and those that are repeated across different cycles, i.e., vertices p where one cycle is in contact with another, both having vertex p .

Consider a weakly simple polygon Q , and let p be a vertex of Q that is repeated in the cycle specifying the boundary ∂Q . This implies that there are four edges of the (counterclockwise) cycle, p_0p , pp_1 , p_2p , and pp_3 , incident on p , all of which lie within a halfplane through p (by local optimality). There are then two subcases: (i) p_0, p, p_1 is a left turn (Figure 9, left); and (ii) p_0pp_1 is a right turn (Figure 9, right). In subcase (i), p_0p, pp_1 define a left turn at p (making p locally convex for Q), and p_2p, pp_3 define a right turn at p (making p locally reflex for Q). In this case, we replace the pair of edges p_0p, pp_1 with a shorter polygonal chain, namely the “taut” version of this path (homotopically equivalent to it), from p_0 to p_1 , along a shortest path, $\beta_{0,1}$, among the polygons Q_i , including Q , treating them as obstacles. The taut path $\beta_{0,1}$ is computed in linear time and consists of left turns only, at (locally convex) vertices of polygons Q_i ($Q_i \neq Q$) or (locally reflex) vertices of Q , where new pinch points of Q are created. Refer to Figure 9, left. Case (ii) is treated similarly; see Figure 9, right. Thus, resolving one repeated vertex, p , of Q can result in the creation of other repeated vertices of Q , or repeated vertices where two cycles come together (discussed below). The process is finite, though, since the total length of all cycles strictly decreases with each operation; in fact, there can be only a polynomial number ($O(n^3)$) of such adjustments, since each triple (p_0, p, p_1) , is resolved at most once.

Now consider a vertex p that appears once as a reflex vertex in Q_1 (with incident ccw edges p_0p and pp_1) and once as a convex vertex in Q_2 (with incident ccw edges p_2p and pp_3). This is because cycles resulting after phase 1 are locally shortest, p must be reflex in one cycle and convex in the other. Our local operation in this case results in a merging of the two cycles Q_1 and Q_2 into a single cycle, replacing edges p_0p (of Q_1) and pp_3 (of Q_2) with the taut shortest path, $\beta_{0,3}$. As in the process described above, this replacement can result in new repeated vertices, as the merged cycle may come into contact with other cycles, or with itself.

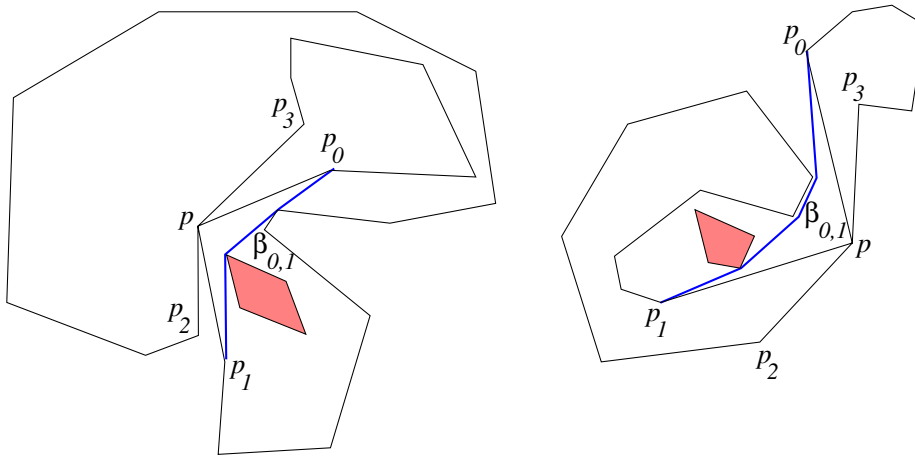


Figure 9: Left: Case (i) of the phase 2 shortening process for a pinch point of Q . Right: Case (ii) of the phase 2 shortening process.

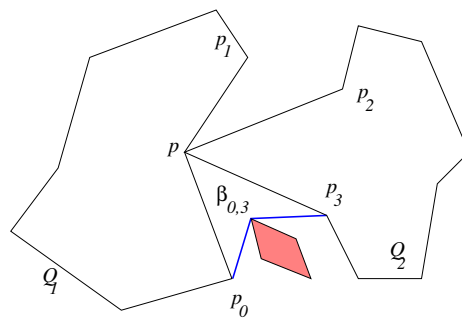


Figure 10: The phase 2 shortening process for a point p shared by cycles Q_1 and Q_2 .

Finally, the result of phase 2, is a set of disjoint cycles, with no repeated vertices, defining disjoint simple polygons within $CH(V)$; these cycles define the holes of the output polygon, whose total perimeter length is at most that of $CH(V)$, plus twice the lengths of the cycles $\gamma(U)$ in an optimal 2-factor of the interior points U . Thus, we obtain a valid solution with objective function at most 3 times optimal. The total running time is polynomial; a straightforward implementation takes time $O(n^4)$, but this time bound can likely be improved substantially. \square

4 IP Formulation

4.1 Cutting-Plane Approach

In the following we develop suitable Integer Programs (IPs) for solving the MP3 to provable optimality. The basic idea is to use a binary variable $x_e \in \{0, 1\}$ for any possible edge $e \in E$, with $x_e = 1$ corresponding to e being part of a solution P if and only if $x_e = 1$. The objective is then to $\min \sum_{e \in E} x_e c_e$, where c_e is the length of e . In addition, we impose a suitable set of linear constraints on these binary variables, such that they characterize precisely the set of polygons with vertex set V . The challenge is to pick a set of constraints that achieve this in a (relatively) efficient manner.

As it turns out (and is discussed in more detail in Section 5), there is a significant set of constraints that correspond to eliminating cycles within proper subsets $S \subset V$. Moreover, there is an exponential number of relevant subsets S , making it prohibitive to impose all of these constraints at once. The fundamental idea of a cutting-plane approach is that much fewer constraints are necessary for characterizing an optimal solution. To this end, only a relatively small subfamily of constraints is initially considered, leading to a relaxation. As long as solving the current relaxation yields a solution that is infeasible for the original problem, violated constraints are added in a piecemeal fashion, i.e., in *iterations*.

In the following, these constraints (which are initially omitted, violated by an optimal solution of the relaxation, then added to eliminate such infeasible solutions) are called *cutting planes* or simply *cuts*, as they remove solutions of a relaxation that are infeasible for the MP3.

4.2 Basic IP

We start with a basic IP that is enhanced with specific cuts, described in Sections 5.2–5.4. We denote by E the set of all edges between two points of V , we denote by \mathcal{C} a set of *invalid cycles*, and we denote by $\delta(v)$ the set of all edges in E that are incident to $v \in V$. Then we optimize over the following objective function:

$$\min \sum_{e \in E} x_e c_e. \quad (1)$$

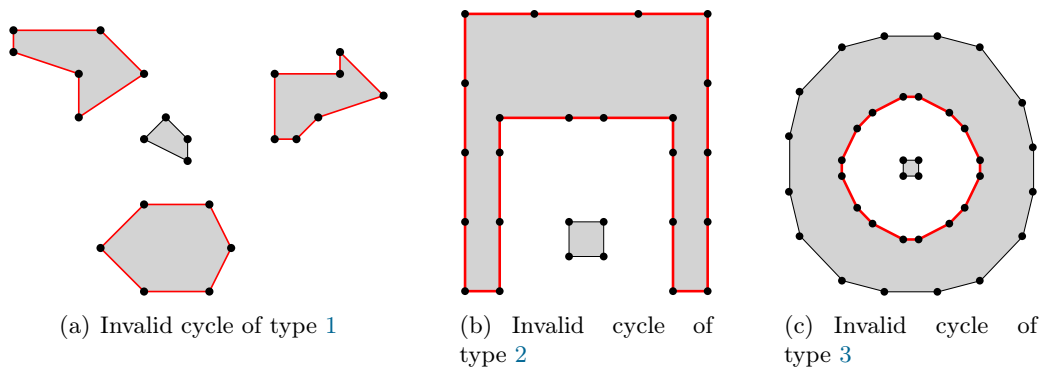


Figure 11: Examples of invalid cycles (red). Black cycles may be valid.

This is subject to the following constraints:

$$\forall v \in V : \sum_{e \in \delta(v)} x_e = 2, \quad (2)$$

$$\forall C \in \mathcal{C} : \sum_{e \in C} x_e \leq |C| - 1, \quad (3)$$

$$x_e \in \{0, 1\}. \quad (4)$$

For the TSP, \mathcal{C} is simply the set of *all* subtours, making identification and separation straightforward. This is much harder for the MP3, where a subtour may end up being feasible by forming the boundary of a hole, but may also be required to connect with other cycles. Therefore, identifying valid inequalities requires more geometric analysis, such as the following. If we denote by CH the set of all convex hull points, then a cycle C is invalid if C contains:

1. at least one and at most $|CH| - 1$ convex hull points. (See Figure 11(a))
2. all convex hull points but does not enclose all other points. (See Figure 11(b))
3. no convex hull point but encloses other points. (See Figure 11(c))

By \mathcal{C}_i we denote the set of all invalid cycles with property i . Because there can be exponentially many invalid cycles, we add constraint (3) in separation steps.

For an invalid cycle with property 1, we use the equivalent cut constraint

$$\forall C \in \mathcal{C}_1 : \sum_{e \in \delta(C)} x_e \geq 2. \quad (5)$$

We use constraint (3) if $|C| \leq \frac{2n+1}{3}$ and constraint (5) otherwise, where $\delta(C)$ denotes the “cut” edges connecting a vertex $v \in C$ with a vertex $v' \notin C$. As argued by Pferschy and Stanek [25], this technique of *dynamic subtour constraints* (DSC) is useful, as it reduces the number of non-zero coefficients in the constraint matrix.

4.3 Initial Edge Set

In order to quickly achieve an initial solution, we sparsify the $\Theta(n^2)$ input edges to the $O(n)$ edges of the Delaunay Triangulation, which naturally captures geometric nearest-neighbor properties. If a solution exists, this yields an upper bound. This technique has already been applied for the TSP by Jünger et al. [19]. In theory, this may not yield a feasible solution: a specifically designed example by Dillencourt shows that the Delaunay triangulation may be non-Hamiltonian [11]; this same example has no feasible solution for the MP3 when restricted to Delaunay edges. We did not observe this behavior in practice.

CPLEX uses this initial solution as an upper bound, allowing it to quickly discard large solutions in a branch-and-bound manner. As described in Section 6, the resulting bounds are quite good for the MP3.

5 Separation Techniques

5.1 Pitfalls

When separating infeasible cycles, the Basic IP may get stuck in an exponential number of iterations, due to the following issues. (See Figures 12–14 for illustrating examples.)

Problem 1: Multiple outer components containing convex hull points occur that (despite the powerful subtour constraints) do not get connected, because it is cheaper to, e.g., integrate subsets of the interior points. Such an instance can be seen in Figure 12, where we have two equal components with holes. Since the two components are separated by a distance greater than the distance between their outer components and their interior points, the outer components start to include point subsets of the holes. This results in a potentially exponential number of iterations.

Problem 2: Outer components that do not contain convex hull points do not get integrated, because we are only allowed to apply a cycle cut on the outer component containing the convex hull points. An outer component that does not contain a convex hull point cannot be prohibited, as it may become a hole in later iterations. See Figure 13 for an example in which an exponential number of iterations is needed until the outer components get connected.

Problem 3: If holes contain further holes, we are only allowed to apply a cycle cut on the outer hole. This outer hole can often cheaply be modified to fulfill the cycle cut but not resolve the holes in the hole. An example instance can be seen in Figure 14, in which an exponential number of iterations is needed.

The second problem is the most important, as this problem frequently becomes critical on instances of size 100 and above. Holes in holes rarely occur on small instances but are problematic on instances of size > 200 . The first problem occurs only in a few instances.

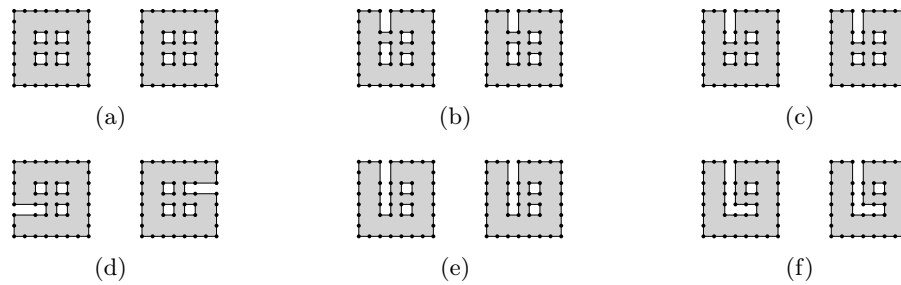


Figure 12: (a) - (f) show consecutive iterations when trying to solve an instance using only constraint (5).

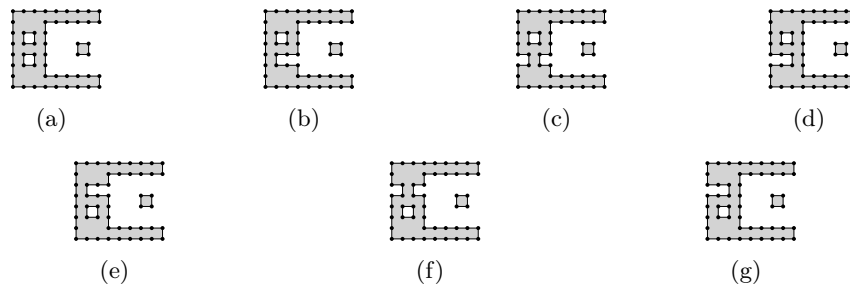


Figure 13: (a) - (g) show consecutive iterations when trying to solve an instance using only constraint (3).

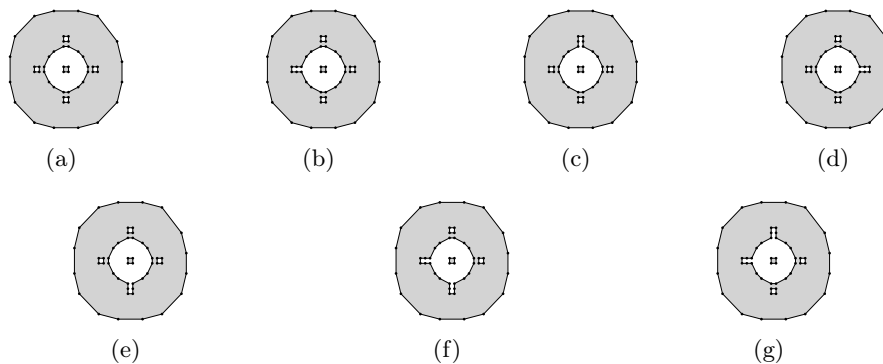


Figure 14: (a) - (g) show consecutive iterations when trying to solve an instance using only constraint (3).

In the following we describe three cuts that each solve one of the problems: The glue cut for the first problem in Section 5.2, the tail cut for the second problem in Section 5.3, and the HiH-Cut for the third problem in Section 5.4.

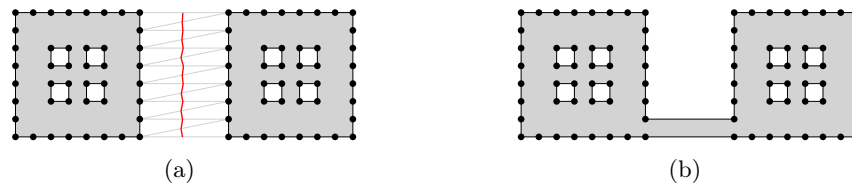


Figure 15: Solving instance from Figure 12 with a glue cut (red). (a) The red curve needs to be crossed at least twice; it is found using the Delaunay Triangulation (grey). (b) The first iteration after using the glue cut.

5.2 Glue Cuts

To separate invalid cycles of property 1 we use *glue cuts* (GC), based on a curve R_D from one unused convex hull edge to another (see Figure 15). With $\mathcal{X}(R_D)$ denoting the set of edges crossing R_D , we can add the following constraint:

$$\sum_{e \in \mathcal{X}(R_D)} x_e \geq 2.$$

Such curves can be found by considering a constrained Delaunay triangulation [6] of the current solution, performing a breadth-first-search starting from all unused convex hull edges of the triangulation. Two edges are adjacent if they share a triangle. Used edges are excluded, so our curve will not cross any used edge. As soon as two different search trees meet, we obtain a valid curve by using the middle points of the edges (see the red curve in Figure 15).

For an example, see Figure 15; as illustrated in Figure 12, this instance is problematic in the Basic IP. This can now be solved in one iteration.

5.3 Tail Cuts

An outer cycle C that does not contain any convex hull points cannot simply be excluded, as it may become a legal hole later. Such a cycle either has to be merged with others, or become a hole. For a hole, each curve from the hole to a point outside of the convex hull must be crossed at least once.

With this knowledge we can provide the following constraint, making use of a special curve, which we call a *tail* (see the red path in Figure 16).

Let R_T be a valid tail and $\mathcal{X}(R_T)$ the edges crossing it. We can express the constraint in the following form:

$$\underbrace{\sum_{e \in \mathcal{X}(R_T) \setminus \delta(C)} x_e}_{\text{C gets surrounded}} + \underbrace{\sum_{e \in \delta(C)} x_e}_{\text{C merged}} \geq 1.$$

The tail is obtained in a similar fashion as the curves of the *Glue Cuts* by building a constrained Delaunay triangulation and doing a breadth-first search starting at the edges



Figure 16: Solving the instance from Figure 13 with a tail cut (red line). (a) The red curve needs to be crossed at least twice or two edges must leave the component. The red curve is found via the Delaunay Triangulation (grey). (b) The first iteration after using the tail cut.

of the cycle. The starting points are not considered as part of the curve and thus the curve does not cross any edges of the current solution.

For an example, see Figure 16; as illustrated in Figure 13, this instance is problematic in the Basic IP. This can now be solved in one iteration. Note that even though it is possible to cross the tail without making the cycle a hole, this is more expensive than simply merging it with other cycles.

5.4 Hole-in-Hole Cuts

The difficulty of eliminating holes in holes (Problem 3) is that they may end up as perfectly legal simple holes, if the outer cycle gets merged with the outer boundary. In that case, every curve from the hole to the convex hull *cannot* cross the used edges exactly two times (edges of the hole are ignored). One of the crossed edges has to be of the exterior cycle, while the other one cannot: otherwise would again leave the polygon. It also cannot be of an interior cycle, as it would have leave to leave that cycle again to reach the hole.

Therefore the inner cycle of a hole in hole either has to be merged, or all curves from it to the convex hull do not have exactly two used edge crossings. As it is impractical to argue over all curves, we only pick one curve P that currently crosses exactly two used edges (see the red curve in Figure 17 with crossed edges in green).

Because we cannot express the inequality that P is not allowed to be crossed exactly two times as an linear programming constraint, we use the following weaker observation. If the cycle of the hole in hole becomes a simple hole, the crossing of P has to change. Let e_1 and e_2 be the two used edges that currently cross P and $\mathcal{X}(P)$ the set of all edges crossing P (including unused but no edges of H). We can express a change on P by

$$\underbrace{\sum_{e \in \mathcal{X}(P) \setminus \{e_1, e_2\}} x_e}_{\text{new crossing}} + \underbrace{(-x_{e_1} - x_{e_2})}_{e_1 \text{ or } e_2 \text{ vanishes}} \geq -1.$$

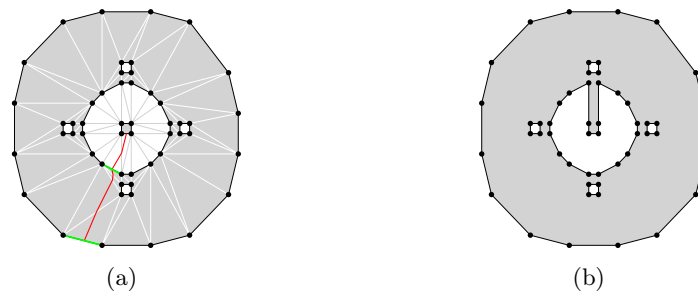


Figure 17: Solving instance from Figure 14 with hole in hole cut (red line). (a) The red line needs to be crossed at least two times or two edges must leave the component or one of the two existing edges (green) must be removed. The red line is built via Delaunay Triangulation. (b) The first iteration after using the hole in hole cut.

Together we obtain the following LP constraint for either H being merged or the crossing of P changing.

$$\underbrace{\sum_{e \in \delta(V_H, V \setminus V_H)} x_e}_{H \text{ merged}} + \underbrace{\sum_{e \in \mathcal{X}(P) \setminus \{e_1, e_2\}} x_e + (-x_{e_1} - x_{e_2})}_{\text{Crossing of } P \text{ changes}} \geq -1.$$

Again we use a breadth-first search on the constrained Delaunay triangulation starting from the edges of the hole in hole. Unlike the other two cuts we need to cross used edges. Thus, we get a shortest path search such that the optimal path primarily has a minimal number of used edges crossed and secondarily has a minimal number of all edges crossed.

For an example, see Figure 17; as illustrated in Figure 12, this instance is problematic in the Basic IP. This can now be solved in one iteration. The corresponding path is displayed in red and the two crossed edges are highlighted in green. Changing the crossing of the path is more expensive than simply connecting the hole in hole to the outer hole and thus the hole in hole gets merged.

6 Experiments

6.1 Implementation

Our implementation uses CPLEX to solve the relevant IPs. Important is also the geometric side of computation, for which we used the CGAL Arrangements package [27]. CGAL represents a planar subdivision using a doubly connected edge list (DCEL), which is ideal for detecting invalid boundary cycles.

6.2 Test Instances

While the TSPLIB is well recognized and offers a good mix of instances with different structure (ranging from grid-like instances over relatively uniform random distribution to

highly clustered instances), it is rather sparse. Observing that the larger TSPLIB instances are all geographic in nature, we designed a generic approach that yields arbitrarily large and numerous clustered instances. This is based on illumination maps: A satellite image of a geographic region at night time displays uneven light distribution. The corresponding brightness values can be used as a random density function that can be used for sampling (see Figure 20). To reduce noise, we cut off brightness values below a certain threshold, i.e., we set the probability of choosing the respective pixels to zero.

6.3 Results

All experiments were run on an *Intel Core i7-4770* CPU clocked at 3.40 GHz with 16 GB of RAM. We set a 30 minute time limit to solve the instances. In Table 1, all results are displayed for every instance that we solved within the time limit. The largest instance solved within 30 minutes is gr666 with 666 points, which took about 6 minutes. The largest instance solved out of the TSPLib so far is dsj1000 with 1000 points, solved in about 37 minutes. In addition, we generated 30 instances for each size, which were run with a time limit of 30 minutes.

Table 1: Runtime in milliseconds of all variants on the TSPLib instances that we solved within 30 minutes. The number in the name of an instance indicates its size.

	BasicIP	+JS+DC +TC+HIHC	+JS+TC +HIHC	+JS+DC +HIHC	+JS+DC +TC	+DC+TC +HIHC
burma14	20	22	17	19	26	19
ulysses16	48	42	35	43	32	42
ulysses22	50	34	55	31	32	61
att48	180	58	72	62	57	129
eil51	74	82	72	78	81	99
berlin52	43	38	37	37	38	51
st70	-	329	324	-	348	414
eil76	714	144	105	530	148	239
pr76	-	711	711	-	731	1238
gr96	376	388	349	10982	384	367
rat99	922	480	485	464	513	1190
kroA100	-	961	689	-	950	1294
kroB100	-	1470	2623	-	1489	2285
kroC100	-	470	431	-	465	577
kroD100	4673	509	451	4334	514	835
kroE100	-	273	273	-	272	574
rd100	-	894	756	-	890	2861
eil101	-	575	445	-	527	1090
lin105	-	390	359	-	412	931
pr107	550	401	272	346	513	923

Continued on next page

Table 1 – Continued from previous page

	BasicIP	+JS+DC +TC+HIHC	+JS+TC +HIHC	+JS+DC +HIHC	+JS+DC +TC	+DC+TC +HIHC
pr124	495	348	264	322	355	940
bier127	439	288	270	267	276	476
ch130	-	1758	1802	-	1594	2853
pr136	1505	964	1029	992	950	3001
gr137	-	1262	1361	-	1252	1724
pr144	6276	1028	2926	985	1030	2012
ch150	-	4938	5167	-	5867	7997
kroA150	-	3427	5615	-	3327	7474
kroB150	-	2993	2396	-	2943	5265
pr152	13285	2161	1619	10978	2151	19479
u159	13285	1424	1262	5339	1410	2513
rat195	106030	16188	19780	77216	16117	27580
d198	-	19329	155550	-	19398	41118
kroA200	-	26360	13093	-	26389	11844
kroB200	-	5492	6239	-	5525	15238
gr202	-	4975	7512	-	4304	9670
ts225	18902	7746	9750	7595	7603	60167
tsp225	91423	11600	9741	28756	11531	44297
pr226	-	8498	2800	-	7204	18848
gr229	-	5462	26478	-	10153	25674
gil262	-	23000	22146	-	-	72772
pr264	24690	6537	-	6719	6549	23641
a280	22023	3601	3857	3980	3619	12983
pr299	-	16251	355323	-	16173	85789
lin318	-	23863	1511219	-	24035	75312
linhp318	-	23107	1313680	-	23064	79352
rd400	-	111128	92995	-	-	302363
fl417	-	198013	-	-	215210	825808
gr431	-	56716	173609	-	78133	265416
pr439	-	46685	36592	-	48231	273873
pcb442	-	1356796	-	-	-	-
d493	-	359072	-	-	-	837229
att532	-	217679	256394	-	218665	817096
ali535	-	93771	427800	-	91828	323104
u574	-	371523	199114	-	-	1010276
rat575	-	417494	191198	-	580320	934988
p654	-	864066	-	-	-	-
d657	-	455378	253374	-	646148	1352747
gr666	-	366157	-	-	670818	-

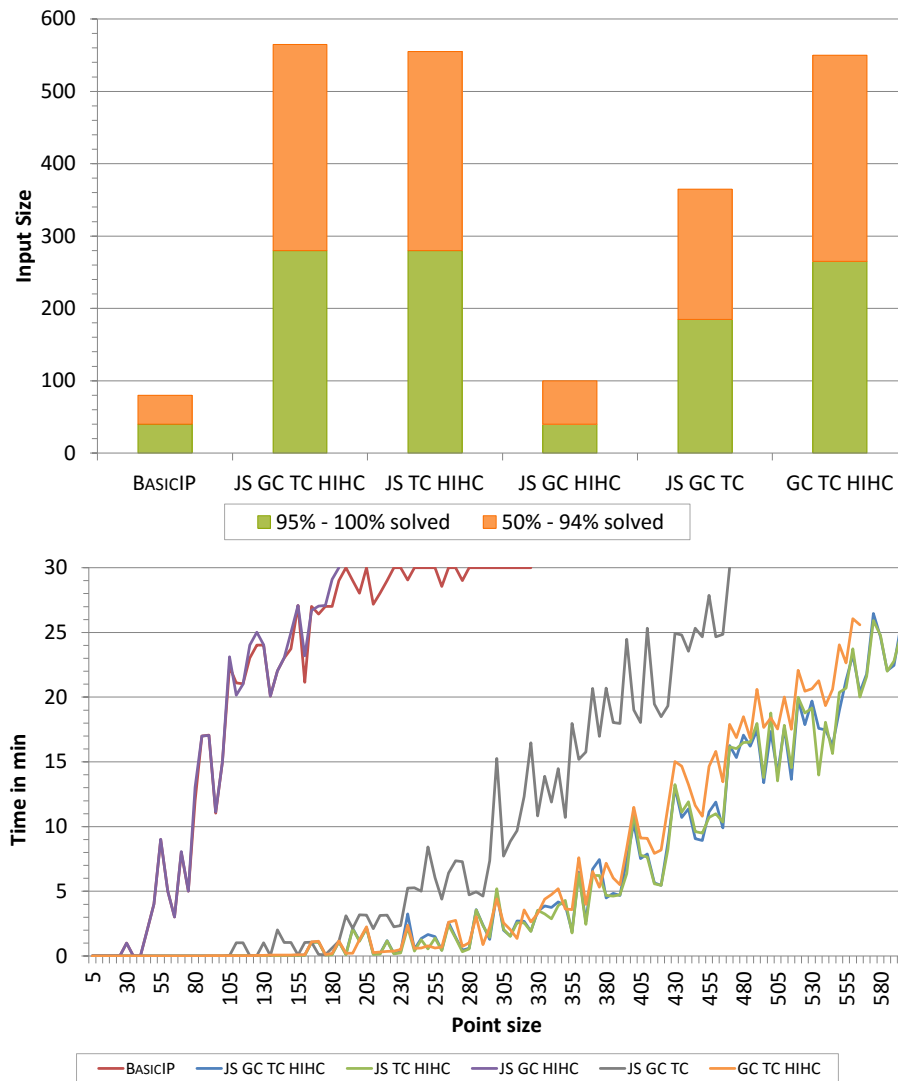


Figure 18: (Top) Success rate for the different variants of using of the cuts, with 30 instances for each input size (*y*-axis). (Bottom) The average runtime of the different variants for all 30 instances. A non-solved instance is interpreted as 30 minutes runtime.

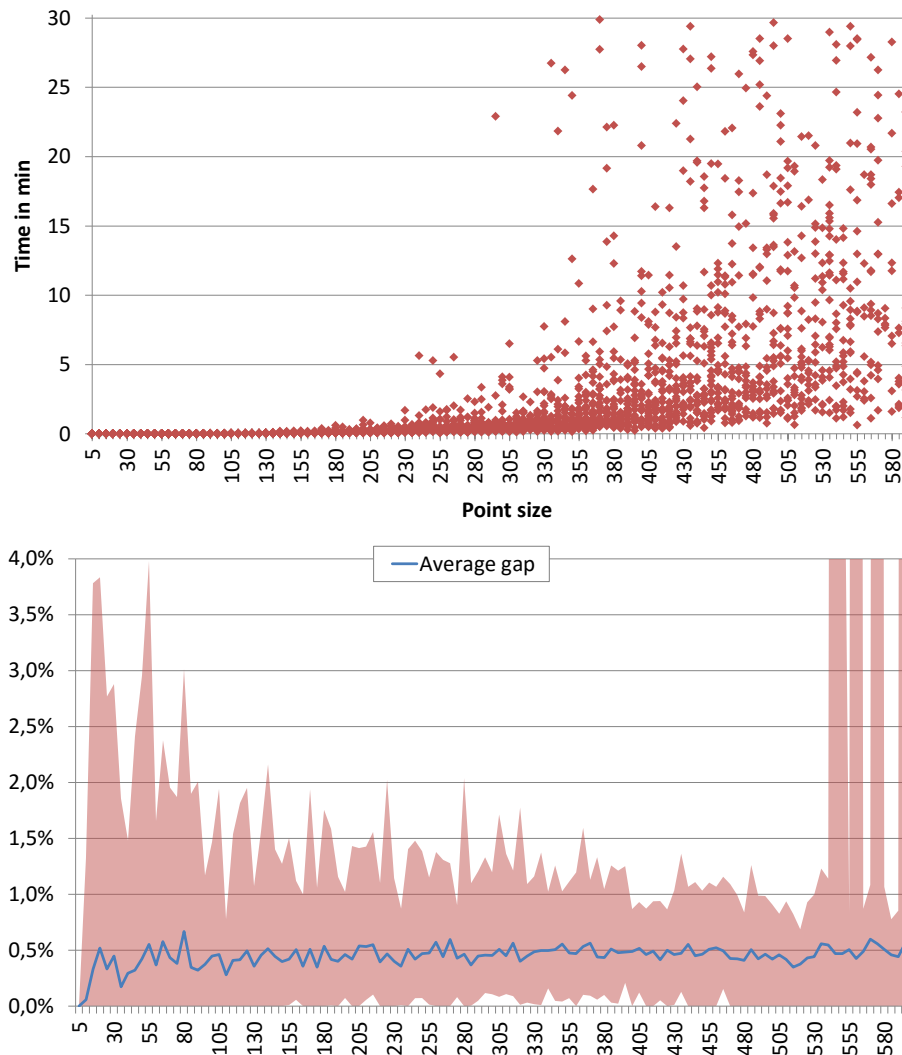
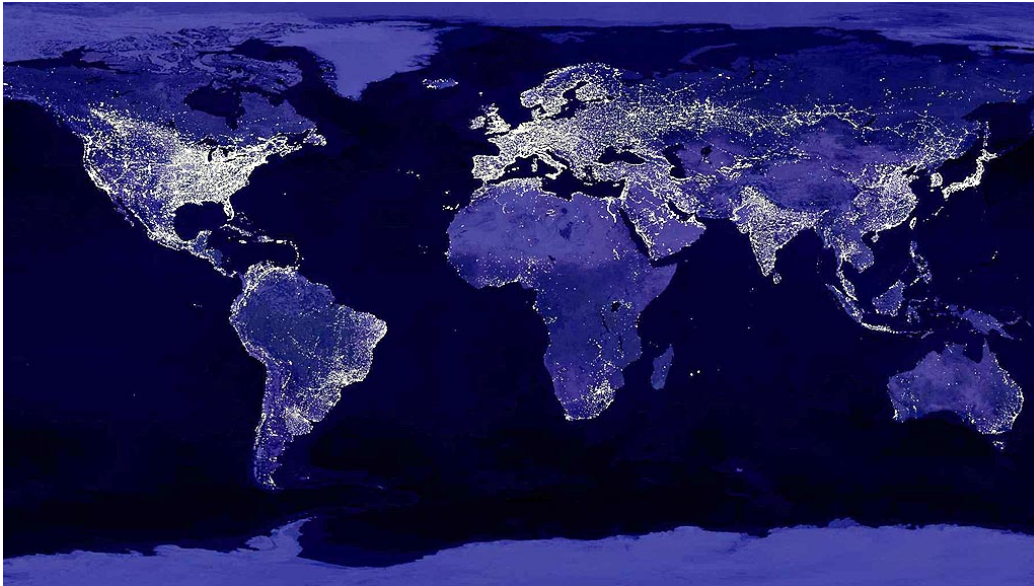


Figure 19: (Top) The distribution of the runtime within 30 minutes for the case of using the jumpstart, glue cuts, tail cuts and HiH-cuts. (Bottom) The relative gap of the value on the edges of the Delaunay triangulation to the optimal value. The red area marks the range between the minimal and maximal gap.



(a) Earth by night



(b) A sampled instance

Figure 20: Using a brightness map as a density function for generating clustered point sets.

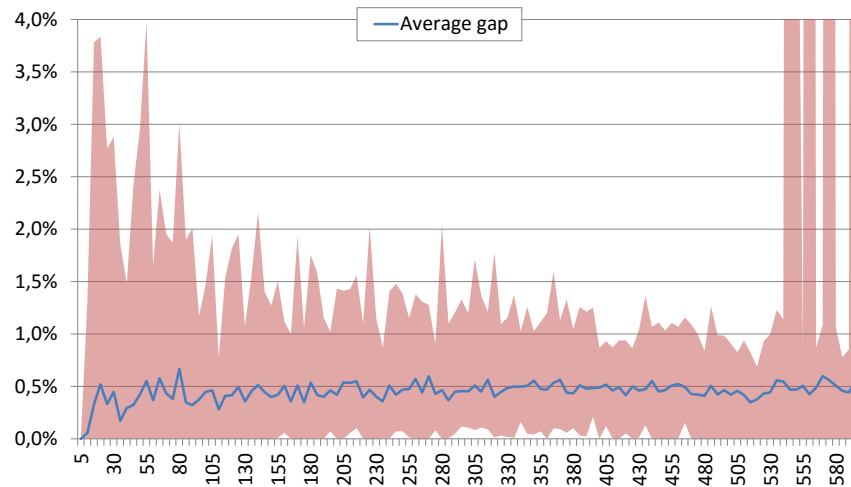


Figure 21: The relative gap of the value on the edges of the Delaunay triangulation to the optimal value. The red area marks the range between the minimal and maximal gap.

We observe that even without using glue cuts and jumpstart, we are able to solve more than 50% of the instances up to about 550 input points. Without the tail cuts, we hit a wall at 100 points, without the HiH-cut instances, at about 370 input points; see Figure 18, which also shows the average runtime of all 30 instances for all variants. Instances exceeding the 30 minutes time limit are marked with a 30-minutes timestamp. The figure shows that using jumpstart shortens the runtime significantly; using the glue cut is almost as fast as the variant without the glue cut.

Figure 19 shows that medium-sized instances (up to about 450 points) can be solved in under 5 minutes. We also show that restricting the edge set to the Delaunay triangulation edges yields solutions that are about 0.5% worse on average than the optimal solution. Generally the solution of the jumpstart gets very close to the optimal solution until about 530 points. After that, for some larger instances, we get solutions on the edge set of the Delaunay triangulation that are up to 50% worse than the optimal solution.

7 Conclusions

As discussed in the introduction, considering general instead of simple polygons corresponds to searching for a shortest cycle cover with a specific topological constraint: one outside cycle surrounds a set of disjoint and unnested inner cycles. Clearly, this is only one example of considering specific topological constraints. Our techniques and results should be applicable, after suitable adjustments, to other constraints on the topology of cycles. We gave a 3-approximation for the MP3; it may be that the approximation can be improved, e.g., based on extending known PTAS techniques for TSP [4, 23] to account for the topological constraints.

There are also various practical aspects that can be explored further. It will be interesting to evaluate the practical performance of the theoretical approximation algorithm, not only from a practical perspective, but also to gain some insight on whether the approximation factor of 3 can be tightened. Pushing the limits of solvability can also be attempted, e.g., by using more advanced techniques from the TSP context. We can also consider sparsification techniques other than the Delaunay edges; e.g., the union between the best known tour and the k -nearest-neighbor edge set ($k \in \{2, 5, 10, 20\}$) has been applied for TSP by Land [20], or (see Padberg and Rinaldi [24]) by taking the union of k tours acquired by Lin's and Kernighan's heuristic algorithm [22].

Acknowledgements

We thank Stephan Friedrichs and Melanie Papenberg for helpful conversations. Parts of this work were carried out at the 30th Bellairs Winter Workshop on Computational Geometry (Barbados) in 2015. We thank the workshop participants and organizers, particularly Erik Demaine. Joseph Mitchell is partially supported by NSF (CCF-1526406). Irina Kostitsyna was supported by the Netherlands Organisation for Scientific Research (NWO) under project no. 639.023.208 and by F.R.S.-FNRS.

References

- [1] E. Althaus and K. Mehlhorn. Traveling Salesman-based curve reconstruction in polynomial time. *SIAM Journal on Computing*, 31(1):27–66, 2001.
- [2] D. L. Applegate, R. E. Bixby, V. Chvátal, and W. J. Cook. On the solution of Traveling Salesman Problems. *Documenta Mathematica – Journal der Deutschen Mathematiker-Vereinigung, ICM*, pages 645–656, 1998.
- [3] D. L. Applegate, R. E. Bixby, V. Chvátal, and W. J. Cook. *The Traveling Salesman Problem: A Computational Study (Princeton Series in Applied Mathematics)*. Princeton University Press, Princeton, NJ, USA, 2007.
- [4] S. Arora. Polynomial time approximation schemes for Euclidean Traveling Salesman and other geometric problems. *Journal of the ACM*, 45(5):753–782, 1998.
- [5] H.-C. Chang, J. Erickson, and C. Xu. Detecting weakly simple polygons. In *26th ACM-SIAM Symposium on Discrete Algorithms (SODA)*, pages 1655–1670. SIAM, 2015.
- [6] L. P. Chew. Constrained Delaunay triangulations. *Algorithmica*, 4(1-4):97–108, 1989.
- [7] N. Christofides. Worst-case analysis of a new heuristic for the Travelling Salesman Problem. Technical Report Report 388, Graduate School of Industrial Administration, CMU, 1976.
- [8] W. J. Cook. *In Pursuit of the Traveling Salesman: Mathematics at the Limits of Computation*. Princeton University Press, Princeton, NJ, USA, 2012.
- [9] W. J. Cook, W. H. Cunningham, W. R. Pulleyblank, and A. Schrijver. *Combinatorial Optimization*. Wiley, 1998.
- [10] T. K. Dey, K. Mehlhorn, and E. A. Ramos. Curve reconstruction: Connecting dots with good reason. *Computational Geometry: Theory and Applications*, 15(4):229–244, 2000.

- [11] M. B. Dillencourt. A non-hamiltonian, nondegenerate Delaunay triangulation. *Information Processing Letters*, 25(3):149–151, 1987.
- [12] S. P. Fekete, S. Friedrichs, M. Hemmer, M. Papenberg, A. Schmidt, and J. Troegel. Area- and boundary-optimal polygonalization of planar point sets. In *European Workshop on Computational Geometry (EuroCG)*, pages 133–136, 2015.
- [13] S. P. Fekete, A. Haas, M. Hemmer, M. Hoffmann, I. Kostitsyna, D. Krupke, F. Maurer, J. S. B. Mitchell, A. Schmidt, C. Schmidt, and J. Troegel. Computing nonsimple polygons of minimum perimeter. In *15th International Symposium on Experimental Algorithms (SEA)*, pages 134–149, 2016.
- [14] M. R. Garey and D. S. Johnson. The rectilinear steiner tree problem is NP-complete. *SIAM Journal on Applied Mathematics*, 32:826–834, 1977.
- [15] J. Giesen. Curve reconstruction, the Traveling Salesman Problem and Menger’s theorem on length. In *15th Symposium on Computational Geometry (SoCG)*, pages 207–216, 1999.
- [16] M. Grötschel. On the symmetric Travelling Salesman Problem: Solution of a 120-city problem. *Mathematical Programming Study*, 12:61–77, 1980.
- [17] G. Gutin and A. P. Punnen. *The Traveling Salesman Problem and Its Variations*. Springer, 2007.
- [18] J. Hershberger and J. Snoeyink. Computing minimum length paths of a given homotopy class. *Computational Geometry: Theory and Applications*, 4:63–98, 1994.
- [19] M. Jünger, G. Reinelt, and G. Rinaldi. The Traveling Salesman Problem. *Handbooks in Operations Research and Management Science*, 7:225–330, 1995.
- [20] A. Land. The solution of some 100-city Travelling Salesman Problems. Technical report, London School of Economics, 1979.
- [21] E. L. Lawler, E. L. Lawler, and A. H. Rinnooy-Kan. *The Traveling Salesman Problem: A Guided Tour of Combinatorial Optimization*. Wiley, 1985.
- [22] S. Lin and B. W. Kernighan. An effective heuristic algorithm for the Traveling-Salesman problem. *Operations Research*, 21(2):498–516, 1973.
- [23] J. S. B. Mitchell. Guillotine subdivisions approximate polygonal subdivisions: A simple polynomial-time approximation scheme for geometric TSP, k -MST, and related problems. *SIAM Journal on Computing*, 28(4):1298–1309, 1999.
- [24] M. Padberg and G. Rinaldi. A branch-and-cut algorithm for the resolution of large-scale symmetric Traveling Salesman Problems. *SIAM Review*, 33(1):60–100, 1991.
- [25] U. Pferschy and R. Staněk. Generating subtour constraints for the TSP from pure integer solutions. Technical report, Department for Statistics and Operations Research, University of Graz, 2014.
- [26] G. Reinelt. TSPLib – A Traveling Salesman Problem library. *ORSA Journal on Computing*, 3(4):376–384, 1991.
- [27] R. Wein, E. Berberich, E. Fogel, D. Halperin, M. Hemmer, O. Salzman, and B. Zukerman. 2D arrangements. In *CGAL User and Reference Manual*. CGAL Editorial Board, 4.3 edition, 2014.